

Low Reynolds Number Propeller Analysis

prepared by: Matthew P. McDowell

Advisor: Professor R.C. Nelson

Department of Aerospace and Mechanical Engineering

University of Notre Dame

Notre Dame, Indiana 46556

August 3, 2010

Abstract

This project was a means of determining the correct way to begin a database of performance characteristics on the low Reynolds number motors and propellers that are used for Notre Dame senior design students. A Kontronik FUN 480-33 Brushless Electronic Motor and APC propellers with an 11.0-inch diameter and 5.5-inch, 7.0-inch, and 8.5-inch pitches were used. Plots of the data obtained of the aerodynamic characteristics of the propellers are included in this paper. A full database can be achieved by varying both the diameter and the pitch, then running the same procedure that is listed below. Potentially, one could have diameters of 7.0-inch, 9.0-inch, 11.0-inch, and 13.0-inch, while varying the pitch of 3.0-inch, 5.5-inch, 7.0-inch, and 8.5-inch for each diameter.

1.0 Introduction

Students have little access to specific performance data on the low Reynolds number motors and propellers that are used for the senior design project. The AME 40452 course at the University of Notre Dame consists of designing an RPV aircraft to complete various flight objectives set by the professor of the course. Previous years' tasks include the separation and docking of mother and daughter aircraft while in flight and horizontal takeoff and flight with a specified payload. In order to properly design the RPV aircraft, performance characteristics of the motor and propeller must be analyzed. The motor used was a Kontronik FUN 480-33 Brushless Electronic Motor, [2] while the propellers used were APC propellers with an 11.0-inch diameter and 5.5-inch, 7.0-inch, and 8.5-inch pitch. By utilizing the plots in this paper, students can obtain information on which size propeller to use for specified flight objectives.

2.0 Method

2.1 Experimental Setup

The experimental setup is identical to that of the AME 30333 Aerodynamics Laboratory course, in which the apparatuses are discussed in Appendix A. Further information on Laboratory setup can be found in *Propeller Characteristics AME 30333 - Experimental Aerodynamics Laboratory Guide - Spring 2009* by Lionel Pittman. The experiment was performed at the University of Notre Dame's Hessert Aerospace Laboratory, using the "Atmospheric Tunnel."

2.2 Procedure

After all of the AME 30333 experimental setup was completed, the following procedure was followed:

1. Zero the offsets of the Manometer Voltage, the Thrust Voltage and the Torque Voltage
2. Turn on the wind tunnel and set the tunnel velocity to the freestream velocity for the first advance ratio (begin with $0m/s$).
3. Turn on the function generator output to the 0% throttle condition.
4. Turn on the power supply.
5. Increase the throttle by increasing the Pulse of the function generator until the frequency of the propeller is approximately 60 Hz.
6. Record the following quantities:
 - manometer voltage
 - voltage supplied to motor
 - current supplied to motor
 - motor RPM
 - voltage from thrust
 - voltage from torque
 - Pulse/throttle setting
7. Increase the throttle to a maximum of approximately 200 Hz, recording these quantities for each increase in throttle (fifteen different throttle speeds were taken between 60 and 200 Hz)
8. Record the same quantities each time the velocity of the tunnel is increased (this wind tunnel's velocity varies from $2 m/s$ to $10 m/s$). Data was taken at 6 different velocities.

3.0 Data Analysis

The ratio of the freestream velocity, V , and the velocity imposed by the rotation of the propeller, $r\omega$, where r is the radius and ω was the angular velocity of the propeller, was defined as the advance ratio, J :

$$J = \frac{V}{nd}, \quad (1)$$

where n was the number of rotations per second and d was the diameter of the propeller. Propeller thrust, power, and torque was non-dimensionalized by certain reference areas multiplied by the dynamic pressure based on the rotational velocity, $\rho(nd)^2$. The thrust and torque values were obtained directly through the strain gages on the thrust stand used in the experiment. Propeller power was calculated by multiplying the angular velocity of the propeller by the torque, $P = \omega Q$. The dimensionless coefficients of thrust, torque and power were defined as:

$$C_T = \frac{T}{\rho n^2 d^4}, \quad (2)$$

$$C_Q = \frac{Q}{\rho n^2 d^5}, \quad (3)$$

$$C_P = \frac{P}{\rho n^3 d^5}, \quad (4)$$

$$= \frac{2\rho n Q}{\rho n^3 d^5}, \quad (5)$$

where

$C_T \equiv$ coefficient of thrust

$T \equiv$ thrust

$\rho \equiv$ density of the surrounding medium

$C_Q \equiv$ coefficient of torque

$Q \equiv$ torque

$C_P \equiv$ coefficient of power

$P \equiv$ power.

The propeller efficiency, η_P , was computed by taking the ratio of the thrust power produced by the propeller to the rotational power provided by the motor [1]:

$$\eta_P = \frac{\text{Thrust Power}}{\text{Rotational Power}} = \frac{TV}{2\pi nQ} = J \frac{C_T}{C_P} \quad (6)$$

The DC motor converts electrical power, $P_e = EI$, where E was voltage and I was current, to the mechanical power consumed by the propeller, P .

The motor efficiency, η_{motor} , was the ratio of these power values:

$$\eta_{motor} = \frac{P}{P_e}, \quad (7)$$

$$= \frac{2\pi nQ}{EI}. \quad (8)$$

In this experiment, the diameter of the propeller remained constant, while the pitch was varied. The standard propeller for the AME 40452 course is an APC 11.0-inch diameter by 7.0-inch pitch. The other pitches used were 5.5-inch and 8.5-inch. In addition, a wooden 11.0-inch diameter by 7.0 inch pitch propeller was used as well. Below are the performance characteristics of the APC 11.0-inch diameter by 7.0-inch pitch, while the three other propeller graphs are included in Appendix B. Each graph is organized by the varying frequencies of the propeller speeds for each freestream velocity used.

The coefficients of thrust (Figures 1, 7, 13, 19) maintain a fairly consistent trend in which the greatest coefficient is the wood propeller, followed by the 8.5-inch, 7.0-inch, and 5.5-inch pitch fiberglass propellers. The plots of Thrust vs. Tunnel Velocity (Figures 5, 11, 17, 23) maintain the same trend as the coefficients of thrust.

The coefficients of power (Figures 2, 8, 14, 20) and torque (Figures 6, 12, 18, 24) remain the greatest for the wood propeller, followed by the 8.5-inch, 7.0-inch, and 5.5-inch pitch fiberglass propellers.

However, the motor efficiencies (Figures 4, 10, 16, 22) seem to challenge this trend. The most efficient motor occurs when using the wood propeller, followed by the 7.0-inch, 5.5-inch, and 8.5-inch pitch fiberglass propellers. Although the 8.5 inch propeller is the most powerful of the fiberglass propellers, it also led to the most inefficient motor.

The propeller efficiencies (Figures 3, 9, 15, 21) differ even more so: the most efficient propeller is the 8.5-inch pitch fiberglass propeller, followed by the 5.5-inch pitch fiberglass propeller, the 7.0-inch pitch fiberglass propeller, and finally the wood propeller.

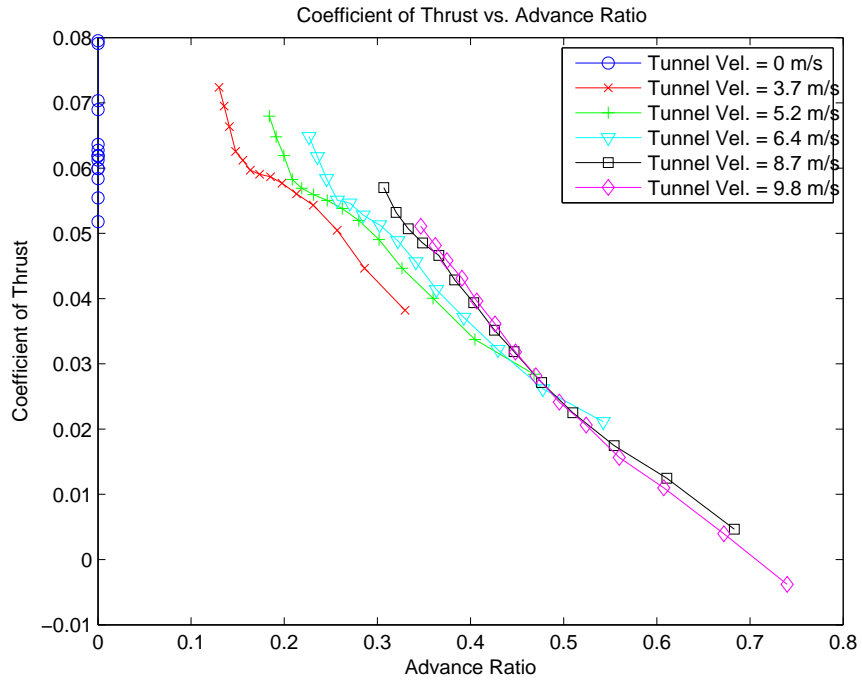


Figure 1: 11in x 7in Fiberglass Prop, Coefficient of Torque vs. Advance Ratio.

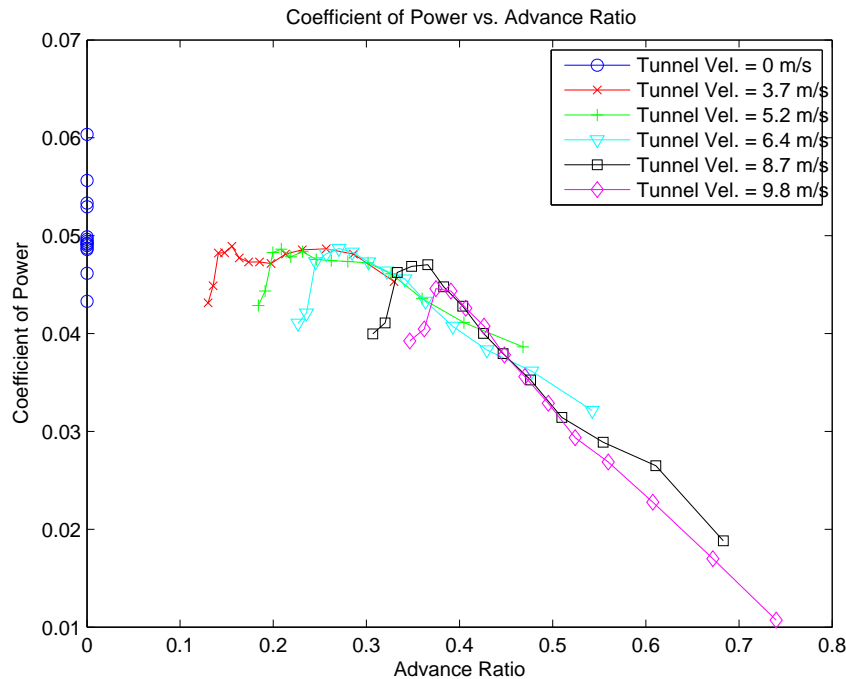


Figure 2: 11in x 7in Fiberglass Prop, Coefficient of Power vs. Advance Ratio.

4.0 Conclusion

Although the 8.5-inch pitch fiberglass propeller was the most powerful of the fiberglass propellers used, it sacrificed the motor efficiency substantially. Completing this database would result in the ability of the students to optimize their aircraft design by utilizing which propeller would best meet the objective at hand by being able to weigh all the aerodynamic characteristics analyzed. In addition to varying the pitch, one improvement would be varying both the diameter and the pitch, then running the same experiments. Potentially, one could have diameters of 7.0-inch, 9.0-inch, 11.0-inch, and 13.0-inch, while varying the pitch of 3.0-inch, 5.5-inch, 7.0-inch, and 8.5-inch for each diameter.

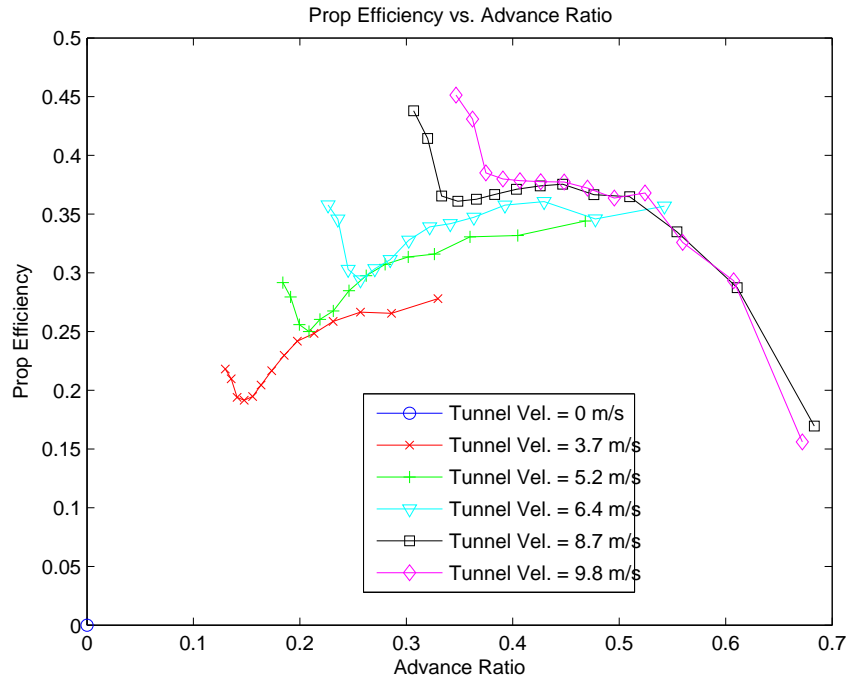


Figure 3: 11in x 7in Fiberglass Prop, Propeller Efficiency vs. Advance Ratio.

Appendix A

Propeller Characteristics Measurement Equipment [1]

The test stand is used to measure the propeller thrust and torque. The wooden part of the test stand strictly serves as a mount for the propeller dynamometer. Two sheet metal covers (one on each side of the dynamometer) isolate and shield the dynamometer sensing units and electrical wiring from the propeller slipstream. The electric motor is securely

attached to a machined aluminum flange with a hose clamp. This is the only support for the motor. A bearing is press fit into the inner diameter of the motor support flange. The inner race of the bearing is pressed onto a cylindrical shaft, which is secured to an aluminum support bracket with a nut, bolt and washer assembly. This flange is then free to rotate about its central axis, so that when the motor is providing torque to the propeller, the flange turns.

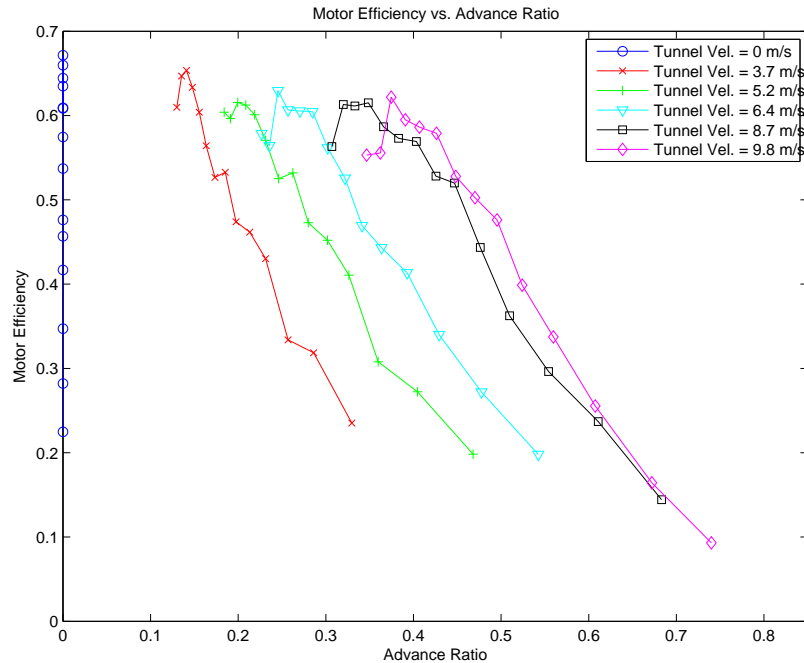


Figure 4: 11in x 7in Fiberglass Prop, Motor Efficiency vs. Advance Ratio.

A thin metal plate is inserted into a slot oriented along the axial direction of the flange. A metal stop is placed on the horizontal part of the aluminum support bracket to stop the plate from continually rotating when the motor shaft is transmitting torque. Four strain gages are applied to the plate to measure the strain exerted on the plate when torque is applied. When properly calibrated, this serves as the method to measure the torque transmitted to the propeller. Two thin metal sheets separate the support bracket from the stationary part of the test stand. These sheets are aligned in the direction of the motor axis and are pinned against opposite sides of the horizontal leg of the bracket with an aluminum bar and two machine screws. When the propeller produces thrust, the entire motor support assembly moves forward and the metal sheets flex. Four strain gages are attached to the rear plate to measure the strain on the plate due to the thrust. With appropriate calibration, this system measures the propeller thrust.

Strain gage arrangement

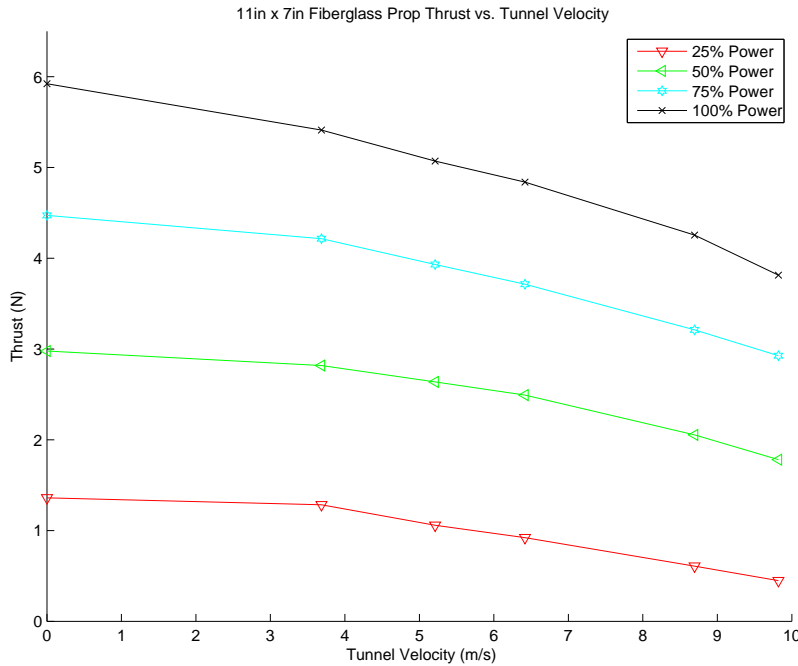


Figure 5: 11in x 7in Fiberglass Prop, Propeller Thrust vs. Tunnel Velocity.

Each plate is equipped with two strain gages on the front and two on the back. Gages are mounted on the front and the back to compensate for temperature effects. Using two gages per side accounts for any lateral difference in the applied strain. Two lead wires (single strand) are soldered between the two gage terminals and two copper terminals for stress relief. Smaller gauge lead wires extend from the copper terminals to the signal conditioning electronics.

Signal conditioning

Each set of four gages is wired into a Wheatstone bridge inside the DMD-520-CC signal conditioning box. The box supplies an excitation voltage across two points of the bridge. The excitation voltage for each channel is adjusted by a screw labeled “Excit”. A multimeter is used to monitor this voltage, which should be near 5V. A second screw labeled “Bal” is used to balance the bridge output voltage to zero when the plate is under no load. When force is applied to a plate, the resistance of each gage on the plate changes and the bridge

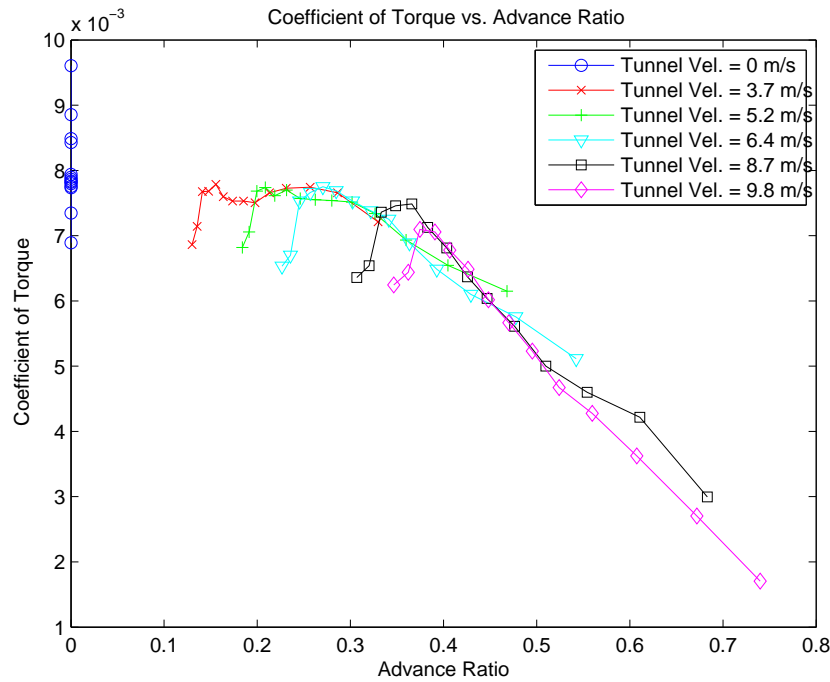


Figure 6: 11in x 7in Fiberglass Prop, Coefficient of Torque vs. Advance Ratio.

becomes unbalanced. This results in an output voltage, which is the base signal for the force. The base signal for each force component is output through a BNC connector on the backside of the box. There is also knob on the back of the box used to adjust the gain of the output signal (1, 100, 200, 500, 1000).

Motor Control

A Tenma 72-630 12V DC power unitsupplies power to the motor. The maximum current that the supply outputs is 24A continuous or 30A for a period of up to 3 minutes (followed by 3 minutes off). The voltage output is adjusted using a knob on the front of the power supply. The power supply signal is pulsed by a Kontronik Jazz 40-16-8 Electronic Speed Controller which allows control of the throttle setting supplied. The pulse signal is controlled using an Agilent 33220A Function/Arbitrary Waveform Generator. This function generator simulates the transmitter and receiver used for R/C aircraft.

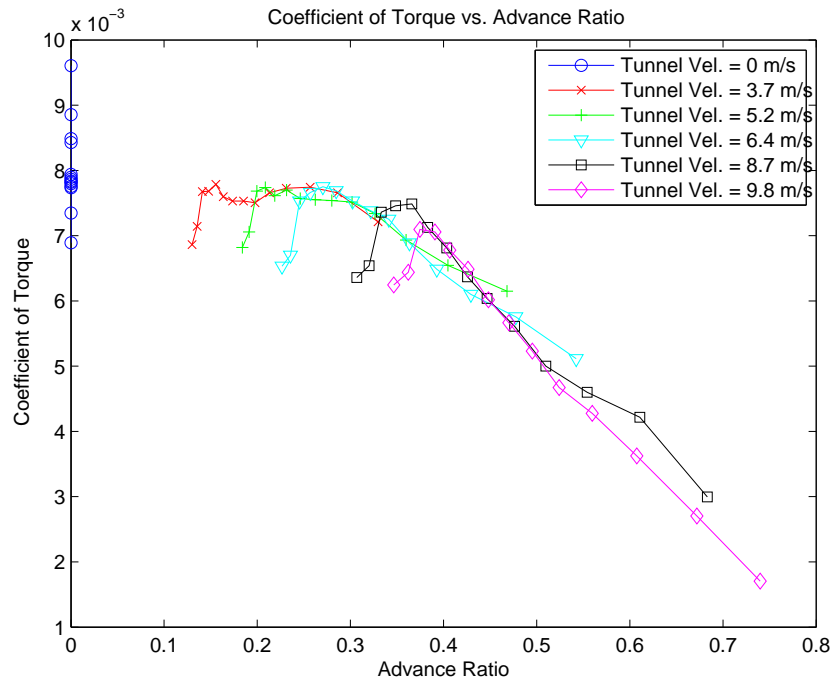


Figure 7: 11in x 7in Fiberglass Prop, Coefficient of Torque vs. Advance Ratio.

Propeller RPM

The propeller RPM is measured using a digital optical tachometer, which sends a voltage pulse each time the propeller passes in front of the optical pickup. The RPM of the propeller is resolved by measuring the frequency of these pulses using an oscilloscope and dividing by the number of propeller blades.

Appendix B

Figures 7-24 below, illustrate the results of varying the pitch of the propeller.

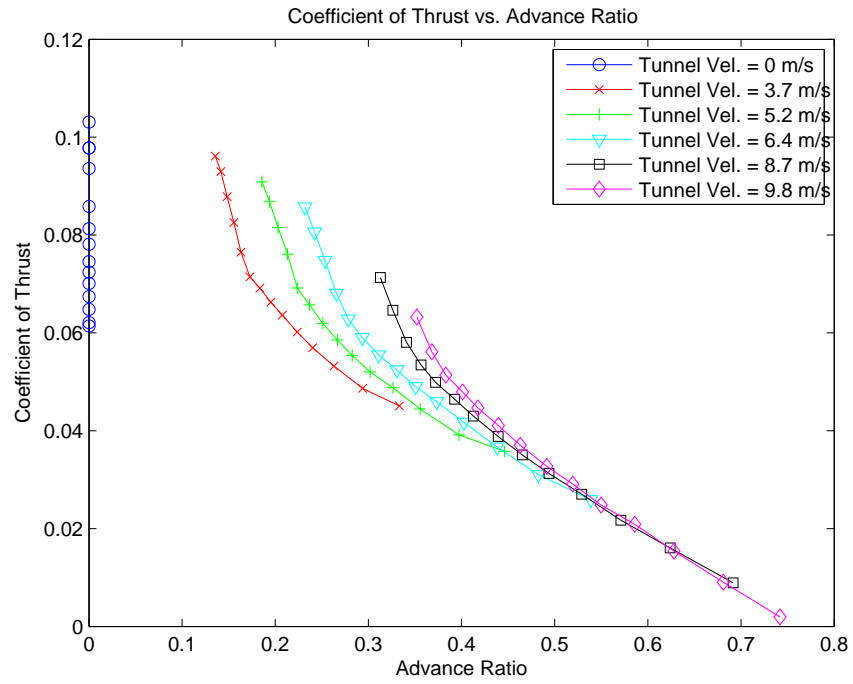


Figure 8: 11in x 7in Wood Prop, Coefficient of Torque vs. Advance Ratio.

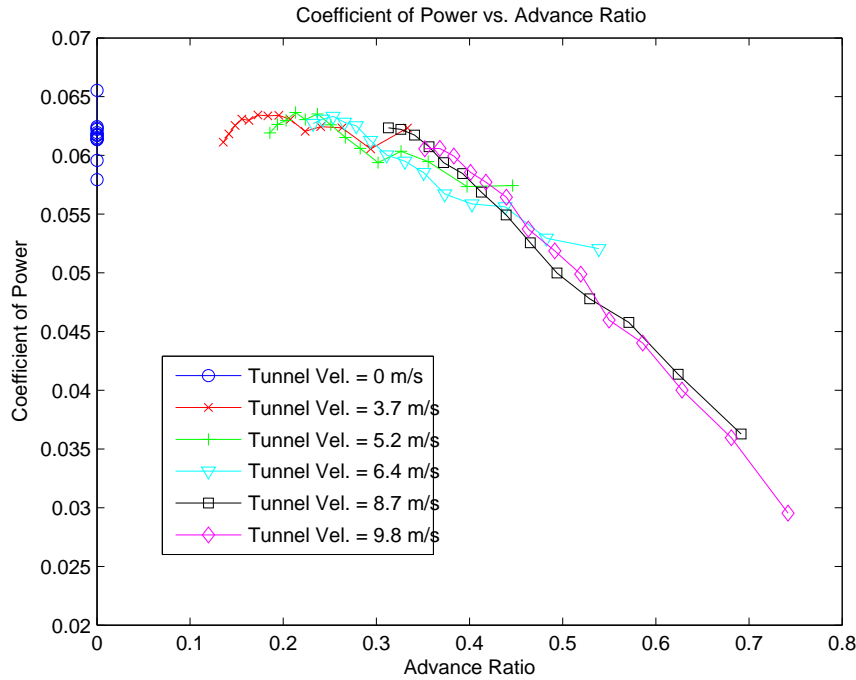


Figure 9: 11in x 7in Wood Prop, Coefficient of Power vs. Advance Ratio.

Appendix C

Two more tests on the propeller were completed: one to check the consistencies of the individual motors and another to specifically use the Spektrum DX7 radio controller. In checking the consistencies of the motors, Motors 1-5 remained consistent within approximately 0.25 N, while Motor 7 (which was recently purchased) provided more thrust than any of the other motors (Figure 25). This newer motor was not subjected to the same wear as the other motors. Motor 6 was not included in this data set because it was inaccessible for the duration of this project. The Spektrum DX7 controller was used to find the maximum thrust of the motor, while demonstrating the 75%, 50%, and 25% thrust values, which the students of the course will be using during their project. The students will use maximum thrust for the takeoff of the RPV aircraft, in which the maximum static thrust obtained was approximately 14.1 N (Figure 26).

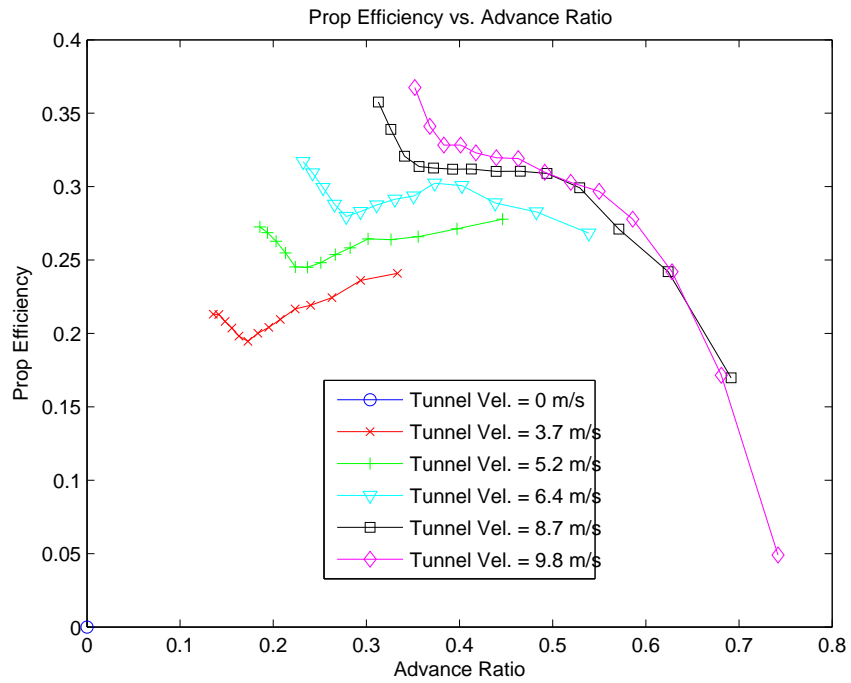


Figure 10: 11in x 7in Wood Prop, Propeller Efficiency vs. Advance Ratio.

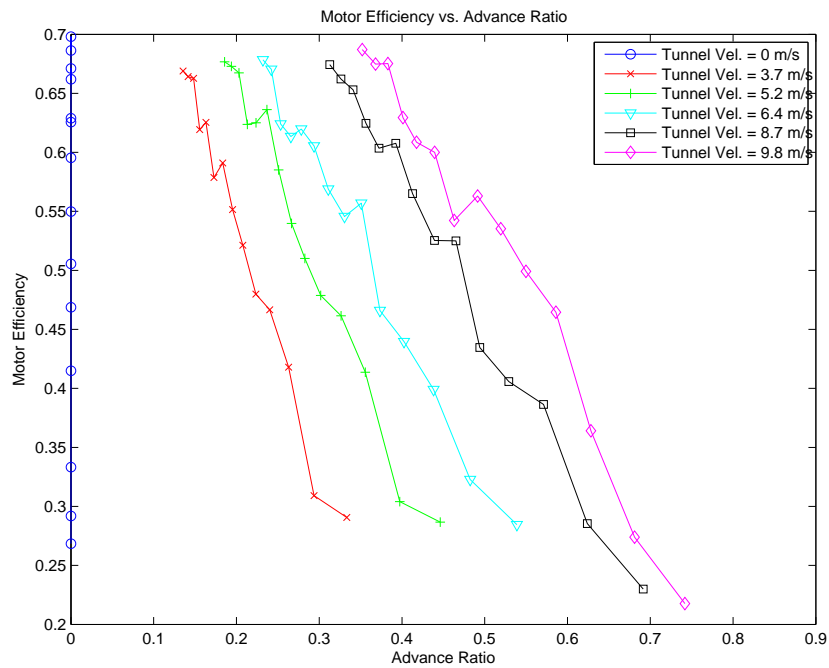


Figure 11: 11in x 7in Wood Prop, Motor Efficiency vs. Advance Ratio.

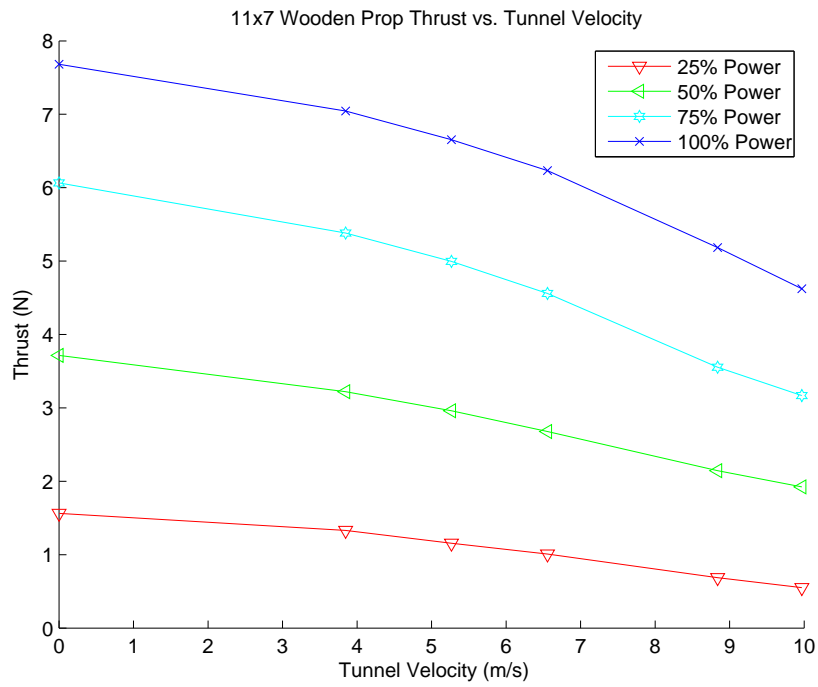


Figure 12: 11in x 7in Wood Prop, Propeller Thrust vs. Tunnel Velocity.

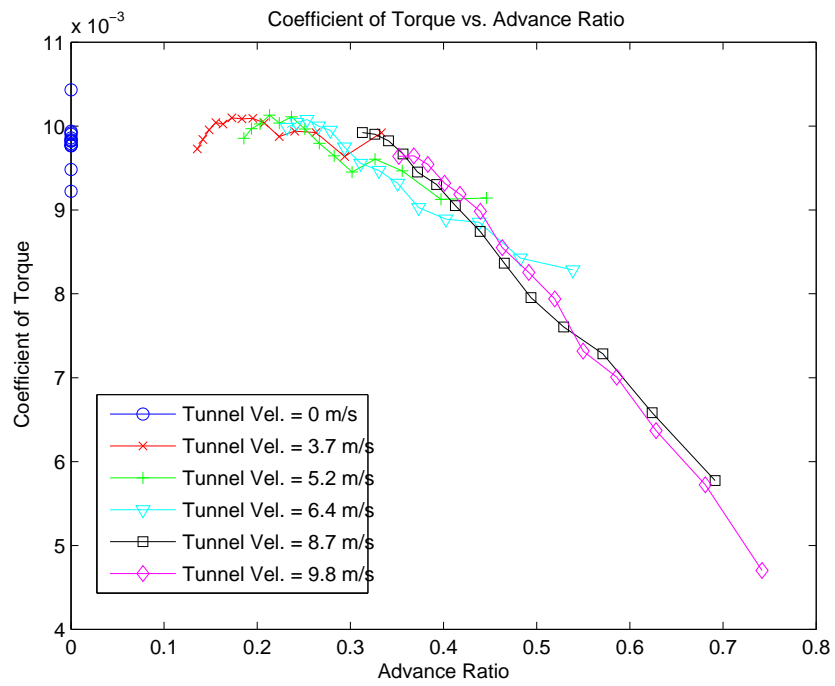


Figure 13: 11in x 7in Wood Prop, Coefficient of Torque vs. Advance Ratio.

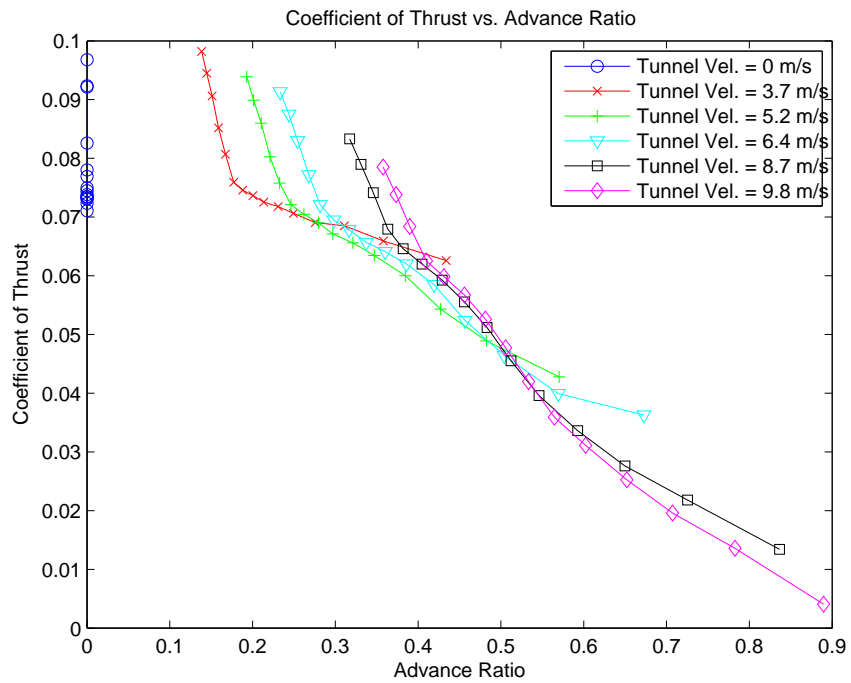


Figure 14: 11in x 8.5 in Fiberglass Prop, Coefficient of Torque vs. Advance Ratio.

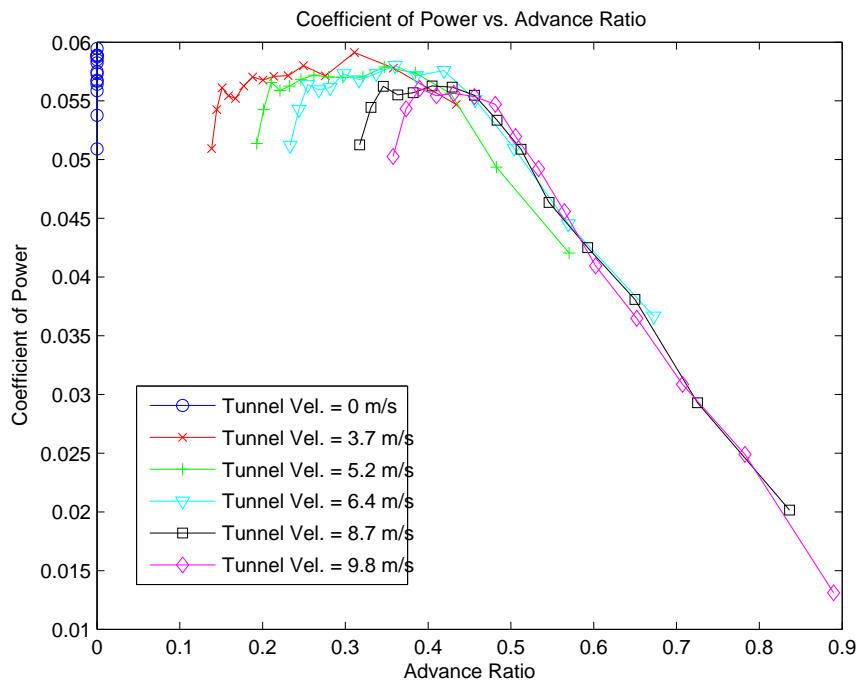


Figure 15: 11in x 8.5 in Fiberglass Prop, Coefficient of Power vs. Advance Ratio.

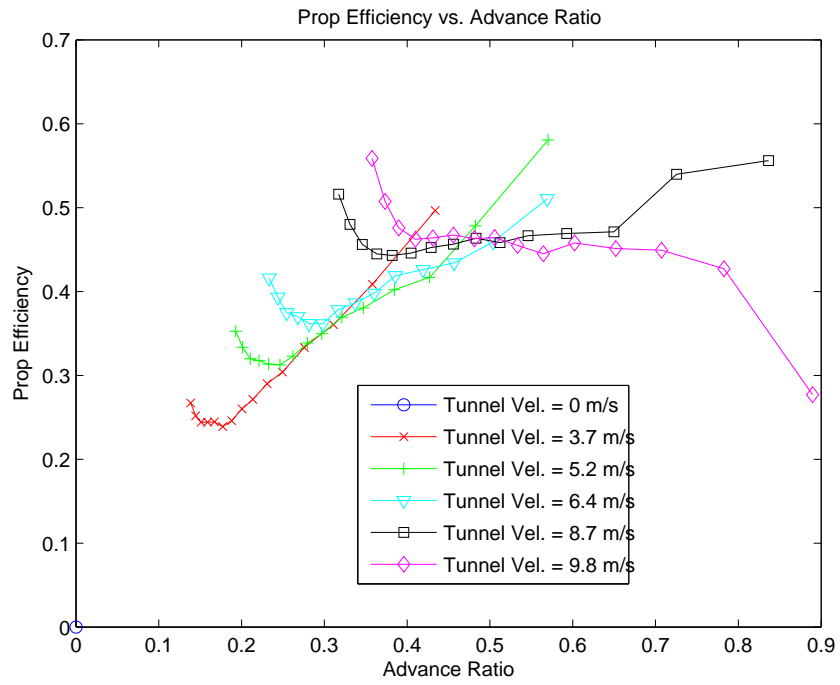


Figure 16: 11in x 8.5 in Fiberglass Prop, Propeller Efficiency vs. Advance Ratio.

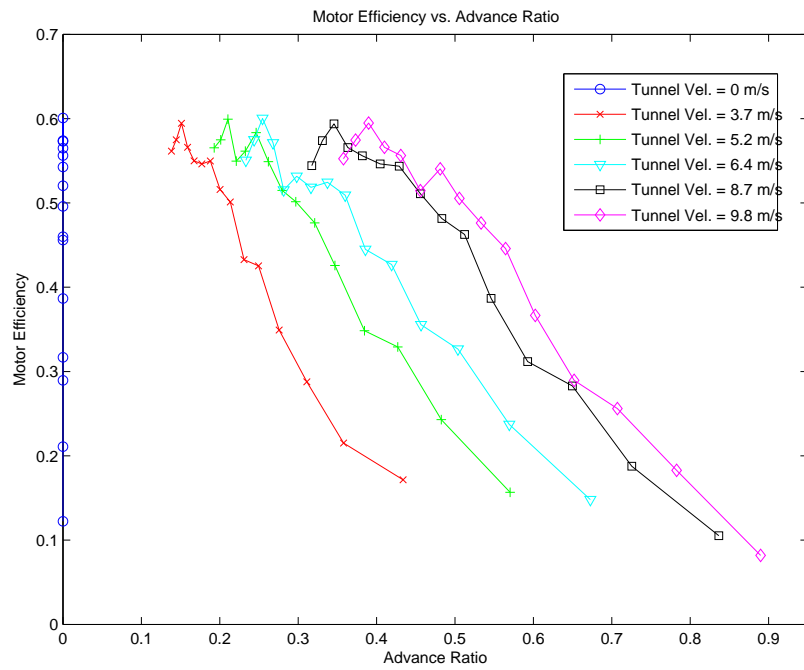


Figure 17: 11in x 8.5 in Fiberglass Prop, Motor Efficiency vs. Advance Ratio.

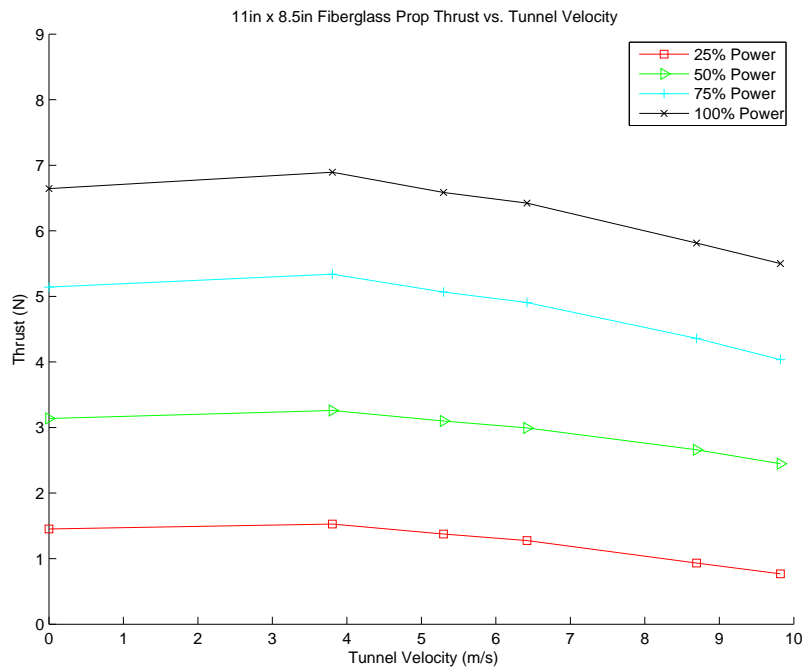


Figure 18: 11in x 8.5 in Fiberglass Prop, Propeller Thrust vs. Tunnel Velocity.

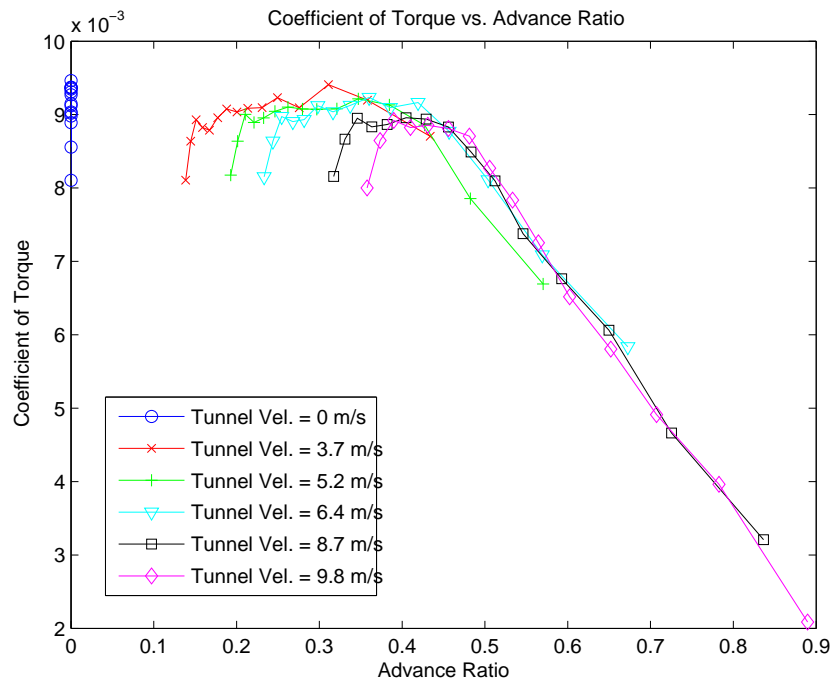


Figure 19: 11in x 8.5 in Fiberglass Prop, Coefficient of Torque vs. Advance Ratio.

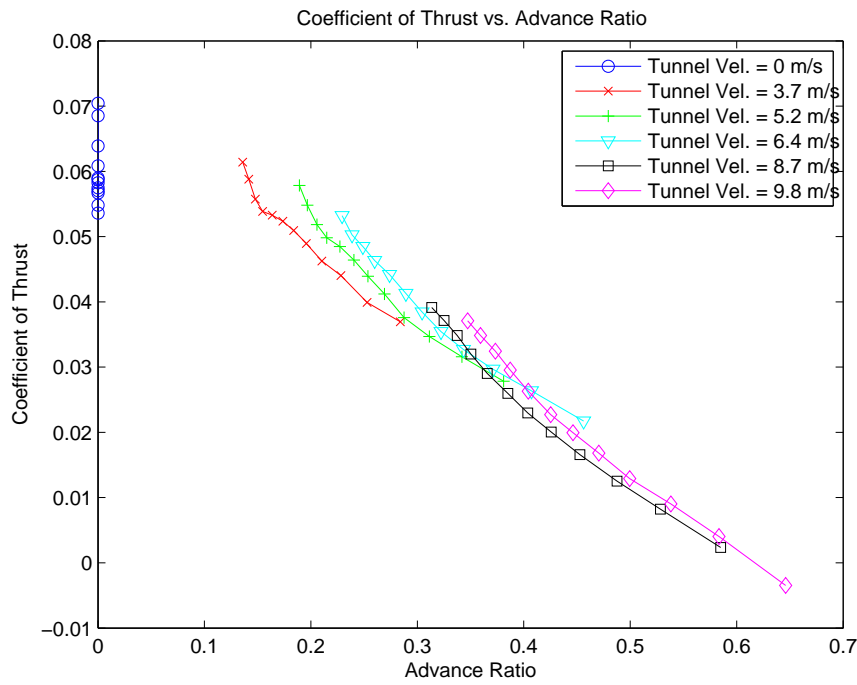


Figure 20: 11in x 5 in Fiberglass Prop, Coefficient of Torque vs. Advance Ratio.

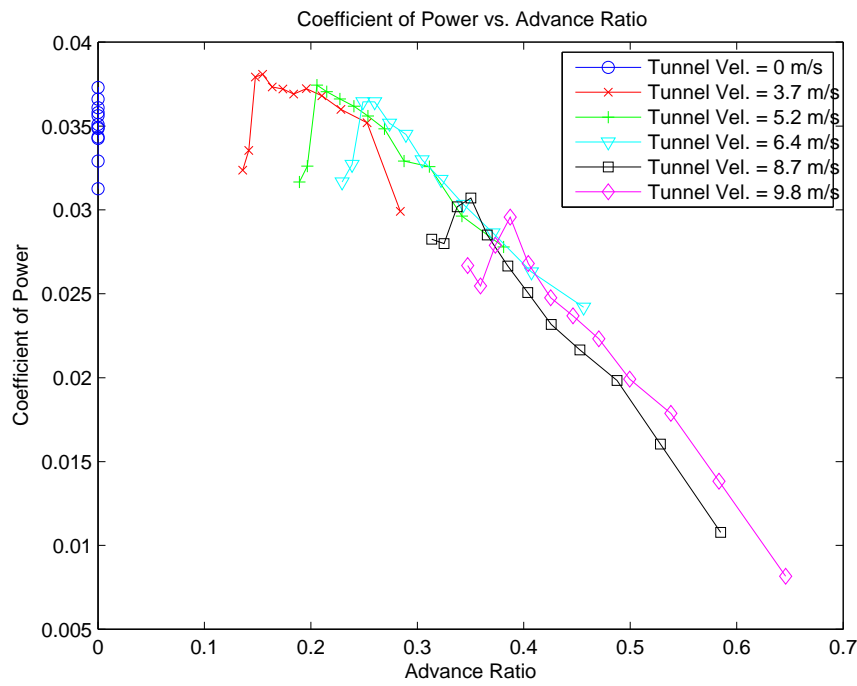


Figure 21: 11in x 5 in Fiberglass Prop, Coefficient of Power vs. Advance Ratio.

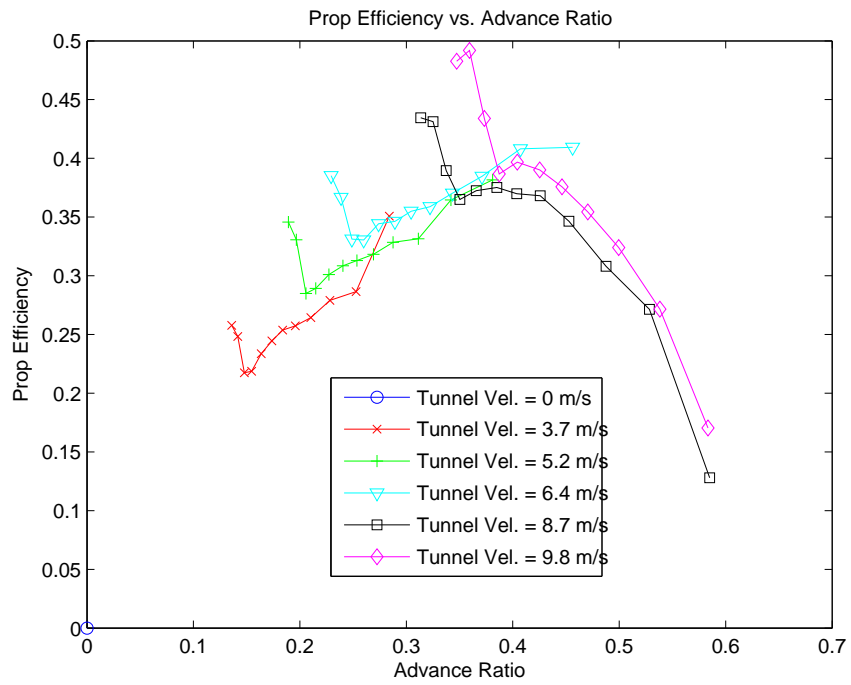


Figure 22: 11in x 5 in Fiberglass Prop, Propeller Efficiency vs. Advance Ratio.

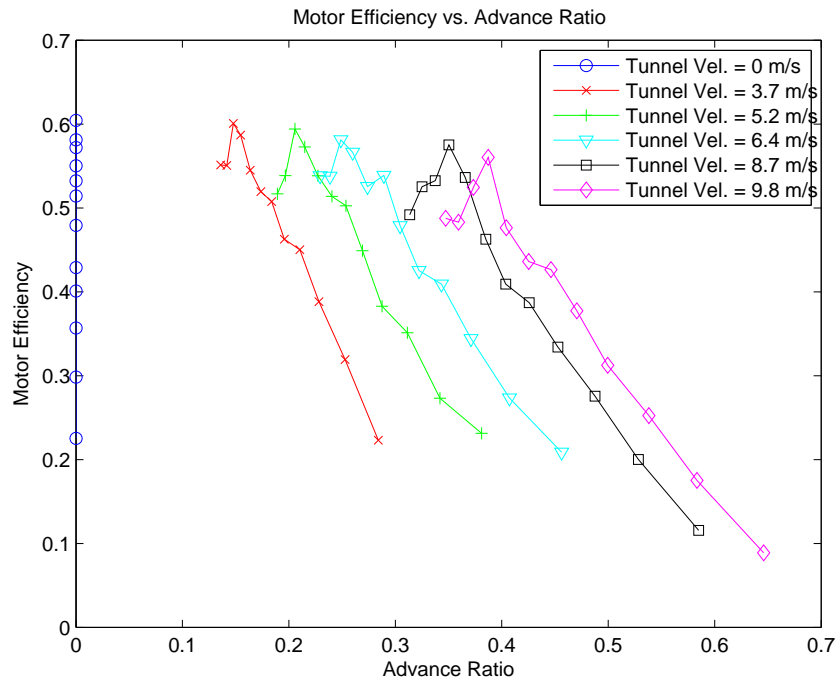


Figure 23: 11in x 5 in Fiberglass Prop, Motor Efficiency vs. Advance Ratio.

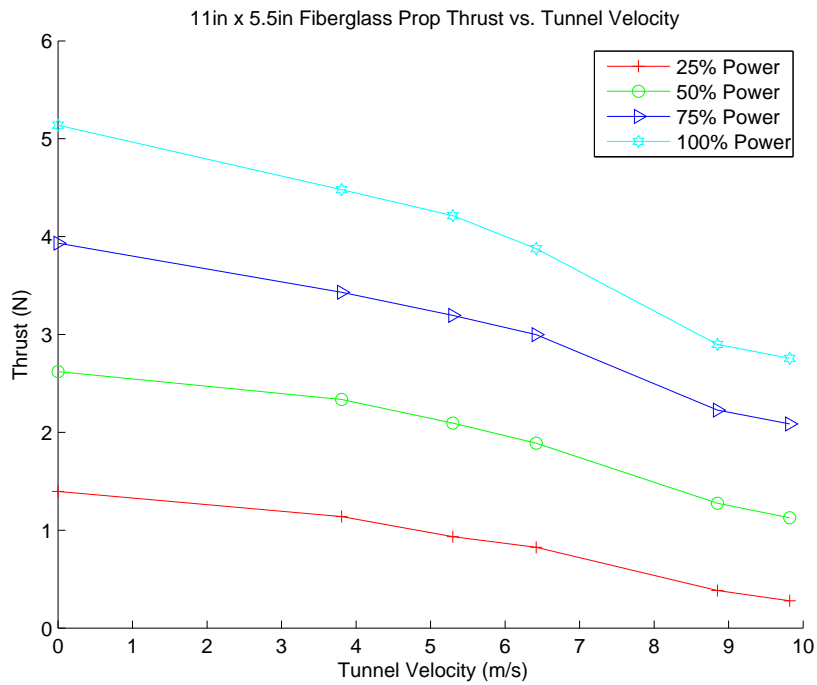


Figure 24: 11in x 5 in Fiberglass Prop, Propeller Thrust vs. Tunnel Velocity.

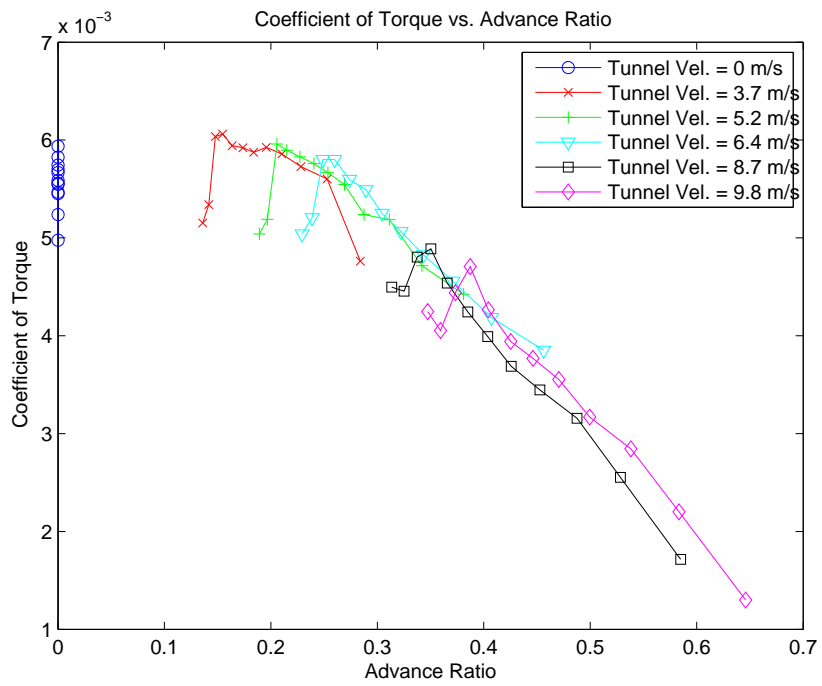


Figure 25: 11in x 5 in Fiberglass Prop, Coefficient of Torque vs. Advance Ratio.

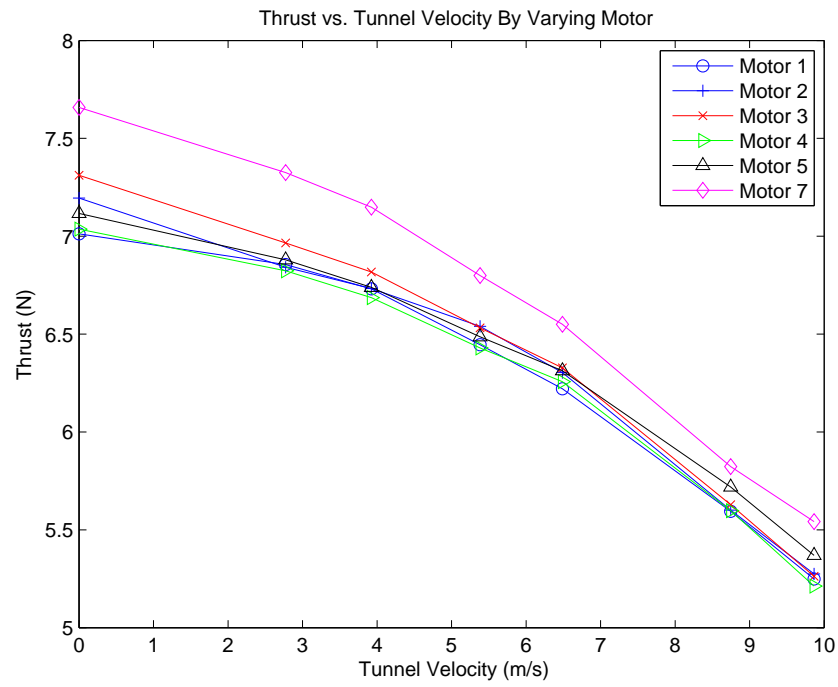


Figure 26: Thrust vs. Tunnel Velocity for each individual motor.

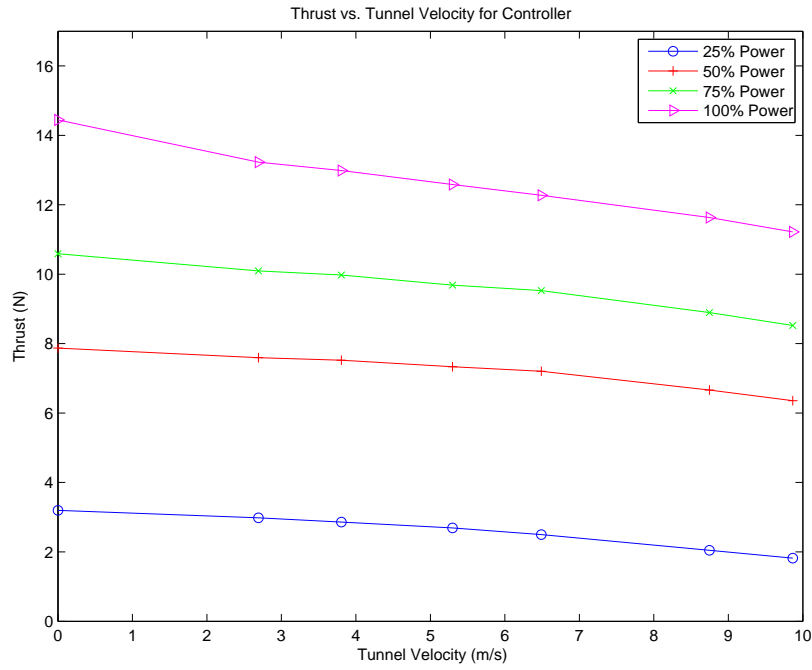


Figure 27: Thrust vs. Tunnel Velocity for DX7 controller.

References

- [1] Pittman, L., 2009, *Propeller Characteristics, AME 30333 - Experimental Aerodynamics Laboratory Guide - Spring 2009, Department of Aerospace and Mechanical Engineering, University of Notre Dame.*
- [2] Shaffer, D. and Turner, M., 2010, *Aerodynamic Prediction for Low Reynolds Numbers, Department of Aerospace and Mechanical Engineering, University of Notre Dame.*